Astron. Astrophys. 347, 212–224 (1999)

ASTRONOMY AND ASTROPHYSICS

# Doppler imaging of stellar surface structure

## X. The FK Comae-type star HD 199178 = V 1794 Cygni

**K.G. Strassmeier**[1,⋆], **S. Lupinek**[1], **R.C. Dempsey**[2,⋆], **and J.B. Rice**[3]

[1] Institut für Astronomie, Universität Wien, Türkenschanzstrasse 17, A-1180 Wien, Austria (strassmeier, lupinek@astro.univie.ac.at)
[2] NASA Johnson Space Center, Code DF25, Houston, TX 77598, USA (robert.c.dempsey1@jsc.nasa.gov)
[3] Department of Physics, Brandon University, Brandon, Manitoba R7A 6A9, Canada (rice@brandonU.ca)

Received 24 November 1998 / Accepted 19 January 1999

**Abstract.** Doppler imaging is used to derive the surface temperature distribution of the FK Comae star HD 199178 for five observing epochs between 1988 and 1997. Our maps are mainly based on Ca I 6439-Å line profiles and simultaneous and contemporary BV and VI photometry. All images of HD 199178 are characterized by a large polar spot and several low-latitude spots with an average surface temperature difference, photosphere minus spots, of 710±260(rms) K for the equatorial spots, ≈1700 K for the polar spot, and 1300±300(rms) K for the polar-spot appendages. The lifetime of some of the low-latitude spots was found to be as short as one month or even less. The lifetime of the polar spot and most of its very cool appendages must exceed the time of our observations, i.e. 9 years or approximately 1000 stellar rotations, and could be as long as 12 years since its discovery by Vogt in 1985. Two consecutive Doppler maps in 1989 show no evidence for differential surface rotation, nor is there substantial evidence for the existence of active longitudes in any of our five images. Instead, we suspect that most of the time variability of the surface features on HD 199178 is short term and possibly chaotic in origin. We conclude that spot lifetimes estimated from the timing of light-curve minima could lead to grossly overestimated lifetimes of individual spots.

With the aid of our optical spectra and the Hipparcos parallax, we redetermine the absolute stellar parameters of HD 199178 and confirm it to be a single G5III-IV star and find 1.65 $M_\odot$ and 11 $L_\odot$ with $T_{\rm eff} \approx 5450$ K, $\log g = 2.5$, and solar abundances.

**Key words:** stars: activity – stars: imaging – stars: individual: HD 199178 – stars: late-type – stars: starspots

### 1. Introduction and scientific goals of this series

One of the most challenging observational goals of today's stellar activity research is to obtain two-dimensional images of inhomogeneous stellar surfaces. Spots cooler than the undisturbed photosphere of a late-type star are a manifestation of surface magnetic fields and a time-dependent study of their latitudinal and longitudinal behavior might provide a link to the stellar dynamo. Our long-term objective is thus to provide conclusive observational constraints for a generalized theory of stellar magnetism as repeatedly suggested, e.g., by Moss et al. (1991) and Landstreet (1992). The near-term goal, however, is to enlarge the available sample of stars with a Doppler map and to investigate the spot morphology as a function of stellar rotation, stellar mass, and evolutionary status. The tenth star to be investigated in this series of papers is the well-known FK Comae star HD 199178 = V1794 Cyg.

HD 199178 (V=$7\overset{\rm m}{.}2$, G5III-IV, $P_{\rm rot}$=3.3 days) belongs to the FK Comae group of rapidly rotating single giants. These stars are located in the Hertzsprung gap of the H-R diagram and have in common strong magnetic activity from the radio to the X-ray wavelengths (e.g., Bopp & Stencel 1981, Bopp et al. 1983, Huenemoerder 1986, Schachter et al. 1996). Because of their rapid rotation, it has been argued that FK Comae-type stars did not evolve from the main sequence as single stars but have evolved from short-period binaries (Bopp & Rucinski 1981, Webbink 1976). Fekel & Balachandran (1993) suggested another scenario in which high angular momentum material is being dredged up to the surface from a rapidly rotating core of a single star. The situation is not settled yet, we are not even sure whether stars like HD 199178 are special objects or just in a rarely observed evolutionary state. Clearly, more detailed observations of these stars are needed to understand FK Comae-type stars.

In this paper we present five new Doppler images of HD 199178 obtained between 1988 and 1997. Sect. 2 describes the photometric and spectroscopic observations. Because the present paper is already the tenth in a series of papers on Doppler imaging of late-type stars, we rediscuss in Sect. 3 some details of our (evolving) mapping technique. In Sect. 4 we obtain the stellar parameters of HD 199178 and in Sect. 5 we present the Doppler maps. Finally, in Sect. 6 we summarize our conclusions.

⋆ Visiting Astronomer, Kitt Peak National Observatory and National Solar Observatory, operated by the Association of Universities for Research in Astronomy, Inc. under contract with the National Science Foundation

## 2. Observations

The spectroscopic observations in this paper were obtained at the Kitt Peak National Observatory (KPNO) and at the National Solar Observatory (NSO). The KPNO observations were made with the coudé feed telescope in May 1990 (dataset "May 1990" in Table 1) and in April 1997 (dataset "April 1997"). In 1990, the 800×800 TI-3 CCD (15$\mu$ pixels) was used with grating A, camera 5, and the long collimator yielding R=24,000 and an effective wavelength resolution of 0.27 Å at $\lambda \approx 6430$ Å. In 1997, the slightly more efficient TI-5 CCD was used with the same grating and camera A but with a narrower slit yielding R=33,000 and a wavelength resolution of 0.20 Å. The NSO observations were part of the synoptic night-time program at the McMath-Pierce telescope during the years 1988 and 1989. Again, a similar 800×800 TI CCD (TI-4 chip, 15 $\mu$ pixels) was used in conjunction with the Milton-Roy grating # 1 to give R=42,000 and an effective wavelength resolution of 0.15 Å. The signal-to-noise ratio is always around 200:1. Table 1 is a summary of the spectroscopic observations (HJD is the heliocentric Julian date, phase is the rotational phase according to Eqs. (1–4) and $\Delta t$ denotes the integration time). Based on previous observations, we felt that the total elapsed time for one image should not exceed approximately 20 days or equivalently six stellar rotations. Consequently, our data were grouped into five sets of 8, 22, 20, 5, and 11 days in length as indicated in Table 1.

All spectroscopic data were reduced with IRAF and included averaged bias subtraction, flat fielding and optimal aperture extraction. Frequent wavelength comparison spectra were obtained throughout the night to guarantee an accurate calibration. The TI CCDs are free of fringing to much below the noise level of our stellar spectra. A representative spectrum of HD 199178 centered at the Ca I 6439-Å line is shown in Fig. 1a.

The new photometric data for April 1997 was obtained with one of the University of Vienna automatic photoelectric telescopes (Amadeus APT; see Strassmeier et al. 1997) at Fairborn Observatory in southern Arizona. The observations were made differentially with respect to SAO 50313 (V = $6\overset{\mathrm{m}}{.}636$, Jetsu et al. 1999b; I = $5\overset{\mathrm{m}}{.}592$, Strassmeier et al. 1999) and filters were selected to match the standard Cousins V(RI)$_C$ system. The 1988–1990 BV photometry from the Phoenix-10 APT was published by Jetsu et al. (1990b), and again analysed in Jetsu et al. (1999b). Additional UBVRI photometry for 1990 was taken from Heckert & Stewart (1992).

**Table 1.** Spectroscopic observations

| Date | HJD (24+) | phase | $\Delta$t (sec) | dataset identification |
|---|---|---|---|---|
| 1988 Aug 03 | 47376.827 | 0.077 | 2400 | August 1988 |
| 05 | 47378.969 | 0.720 | 2400 | August 1988 |
| 09 | 47382.895 | 0.900 | 1500 | August 1988 |
| 10 | 47383.827 | 0.180 | 1800 | August 1988 |
| Nov 28 | 47493.750 | 0.210 | 3300 | ... |
| 29 | 47494.753 | 0.512 | 4200 | ... |
| Dec 14 | 47509.712 | 0.007 | 3900 | ... |
| 18 | 47513.714 | 0.209 | 4400 | ... |
| 1989 Apr 10 | 47627.005 | 0.252 | 1800 | April 1989 |
| 11 | 47627.943 | 0.534 | 2400 | April 1989 |
| 28 | 47644.989 | 0.729 | 2400 | April 1989 |
| 30 | 47646.967 | 0.325 | 2700 | April 1989 |
| May 01 | 47647.980 | 0.630 | 2400 | April 1989 |
| 02 | 47648.987 | 0.933 | 1800 | April 1989 |
| 25 | 47671.936 | 0.840 | 2400 | May–Jun 1989 |
| 27 | 47673.986 | 0.457 | 2100 | May–Jun 1989 |
| 29 | 47675.981 | 0.058 | 1500 | May–Jun 1989 |
| Jun 03 | 47680.971 | 0.560 | 2100 | May–Jun 1989 |
| 04 | 47681.919 | 0.845 | 2700 | May–Jun 1989 |
| 11 | 47688.915 | 0.951 | 3000 | May–Jun 1989 |
| 13 | 47690.851 | 0.534 | 2400 | May–Jun 1989 |
| 23 | 47700.981 | 0.583 | 1800 | ... |
| 25 | 47702.719 | 0.106 | 2700 | ... |
| Jul 13 | 47720.858 | 0.566 | 2400 | ... |
| 14 | 47721.765 | 0.839 | 3600 | ... |
| 1990 May 15 | 48026.917 | 0.756 | 2700 | May 1990 |
| 16 | 48027.937 | 0.064 | 2500 | May 1990 |
| 17 | 48028.946 | 0.369 | 4400 | May 1990 |
| 18 | 48029.925 | 0.664 | 4000 | May 1990 |
| 19 | 48030.840 | 0.940 | 3800 | May 1990 |
| 1997 Apr 06 | 50545.002 | 0.280 | 3600 | April 1997 |
| 07 | 50545.998 | 0.579 | 3000 | April 1997 |
| 08 | 50546.993 | 0.878 | 3600 | April 1997 |
| 09 | 50547.996 | 0.180 | 3600 | April 1997 |
| 10 | 50549.001 | 0.482 | 3400 | April 1997 |
| 11 | 50549.907 | 0.754 | 3600 | April 1997 |
| 12 | 50550.991 | 0.080 | 3600 | April 1997 |
| 13 | 50551.995 | 0.381 | 3600 | April 1997 |
| 14 | 50552.921 | 0.659 | 3600 | April 1997 |
| 15 | 50553.911 | 0.957 | 3600 | April 1997 |
| 16 | 50554.944 | 0.267 | 3600 | April 1997 |

## 3. Data preparation, atomic input data, and mapping procedure

### *3.1. Line-profile preparation for Doppler imaging*

Once the rotational phases of the spectra are known, we extract the mapping line profiles from each spectrum in the proper sequence. Since HD 199178 is a single star, it represents the simplest possible case at this stage of data preparation – there are no radial velocity variations nor depressions of the spot signatures due to the continuum of a secondary star.

Our next step is to remove the instrumental profile from each of the extracted profiles. This is done with a Gaussian approximation to the true instrumental profile. We adopt the average nightly FWHM of several weak lines from a Th-Ar comparison lamp as the FWHM of the instrumental profile. Furthermore, we remove the very high frequency noise much above the Nyquist frequency (based on the instrumental profile) by using a filter determined from the FWHM of the instrumental profile in diodes at the sample spacing in the original stellar spectrum. The noise removal is done before the instrumental profile is removed (see Gray 1992). This procedure is more accurate since the convolution in the forward process would be done in the data

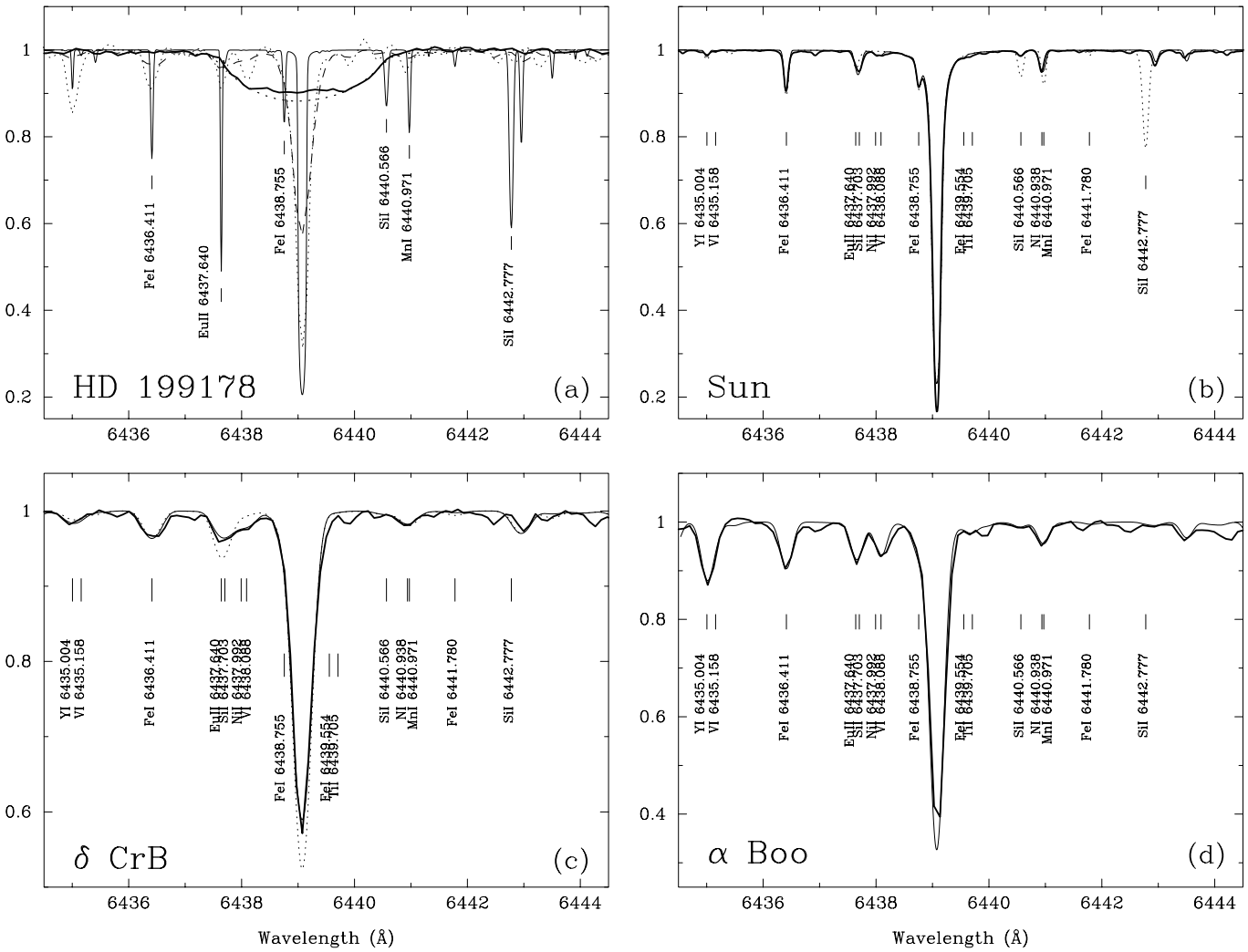


**Fig. 1a–d.** A comparison of observed and synthesized spectra in the Ca I 6439-Å line region. **a** A spectrum of HD 199178 (thick line) compared with the reference stars $\delta$ CrB (G5III-IV; dashed line) and $\alpha$ Boo (K1.5III; dotted line). A broadened synthetic Ca I profile, computed from a $T_{\rm eff}$=5500/$\log g$=2.5 model atmosphere and our revised $\log gf$'s, is shown as a thick dotted line while the unaltered and unbroadened spectrum is shown as a thin full line. **b** A spectrum of the Sun (thick line) and two fits with Kurucz's (1991) solar model with (thin full line) and without (dotted line) modified transition probabilities. **c** The observed spectrum of $\delta$ CrB (thick line) and two fits with solar abundances (dotted line) and adjusted elemental abundances (thin full line), respectively. **d** A spectrum of $\alpha$ Boo = Arcturus (thick line) and the fit with revised abundances (thin line).

domain (not in the Fourier domain) and since the data points are always very widely spaced compared to the instrumental profile, sampling for the convolution would have to involve some interpolation which would be somewhat ad hoc.

### *3.2. Spectrum synthesis of the 6439-Å wavelength region*

Unruh & Collier-Cameron (1995) demonstrated that neglecting blends in the wings of the primary mapping line will lead to spurious banding in the reconstructed image. These artificial bands could show up at higher latitudes the further a blend is away from the mapping-line center. From detailed simulations, Unruh & Collier-Cameron estimate that the ratio of wavelength displacement of the blend to the $v \sin i$ of the star had to be of the order of 1/3 for artifacts to appear.

Our approach to handling this problem is to synthesize a strip of spectrum that includes all known line blends down to an equivalent width of 3 mÅ. This spectrum is then used for the inversion instead of a single line profile. Thus, all the blends will be mapped simultaneously with the dominant main mapping line (Ca I 6439 Å in our case). This requires knowledge of the correct line transition probabilities ($\log gf$-values) for each included blend and we first fit a very high resolution spectrum of the Sun ($\lambda/\Delta\lambda \approx 600{,}000$; Delbouille et al. 1973) with Kurucz's (1991) own solar model at the wavelengths of our interest (Fig. 1b), and then revise the tabulated transition probabilities from Kurucz (1993) if necessary. Table 2 is a list of the adopted transition probabilities for the lines marked in Fig. 1.

Fig. 1a–d summarizes the results from such a synthesis analysis based on pretabulated ATLAS-9 model atmospheres and

an updated line-synthesis program written in Ada (Stift 1995) which is based on the original code by Baschek et al. (1966). A fit to the spectrum of the cool star Arcturus (K1.5III, Peterson et al. 1993), having an effective temperature similar to the average spot temperature on HD 199178, is used to modify the $\log gf$'s for the temperature-sensitive lines that do not show up properly in the solar spectrum, mostly from vanadium, but also to verify the revised $\log gf$'s from the solar fit for a cooler and lower-gravity atmosphere. We thereby slightly modify some of the elemental abundances (Eu, V, and Si) determined by Peterson et al. (1993). A final consistency check is made by fitting the spectrum of a normal M-K standard star that might represent the unspotted photosphere of HD 199178; in our case we used $\delta$ CrB (G5III-IV Fe-1, $[Fe/H] = -0.04$, Keenan & McNeil 1989). We emphasize though that HD 199178 lies in the Hertzsprung gap, where it is difficult to find a star with a spectrum that can be termed "normal" (see Keenan & McNeil 1989). The $\delta$ CrB fit is shown separately in Fig. 1c. $\delta$ CrB is a mildly chromospherically active, single star and a rotationally modulated light variable with a period of around 60 days (Fernie 1991, Choi et al. 1995). It is also somewhat metal deficient, and several new abundances were estimated in the course of this work (using only the spectral range shown in Fig. 1). We found $\log n$(Ca) = 6.00±0.05, $\log n$(Fe) = 7.55±0.03, $\log n$(V) = 4.85±0.05 and $\log n$(Eu) = 0.45±0.02 (based on $\log n$(H) = 12.00).

The most noticeable wrongly synthesized lines in Fig. 1 are the Si I lines at 6440.566 and 6442.777 Å. Further, the observed spectrum of $\delta$ CrB shows some very weak lines that can not be synthesized properly (e.g. Ti I 6439.705 and Ce I 6439.964 Å ) while the unblended Fe I 6436.411 line is clearly seen in $\delta$ CrB and in our synthetic spectrum but is apparently absent, or much weaker, in HD 199178. Only the Eu II 6437.640 + V I 6438.088 blend seems to be present in all spectra in Fig. 1 having a combined equivalent width of 19 mÅ in the synthesized HD 199178 spectrum and 25 mÅ in the $\delta$ CrB spectrum.

Finally, the referee brought to our attention the problem of gravitational darkening of a rotationally deformed star (see Hatzes et al. 1996). In principle, it introduces a temperature gradient from pole to equator, the poles being slightly hotter than the equator, that possibly mimics an equatorial belt of cool spots. If we adopt von Zeipel's (1924) gravity darkening law and its extention to stars with a convective envelope (Lucy 1967), we find a temperature difference between pole and equator for HD 199178 of 120 K. This transforms into a change of equivalent width in our Ca I mapping line of 5–6% from pole to equator. We believe that such a small change is below our temperature resolution and remains burried in the $v \sin i$ modelling. However, we caution the reader that the recovery of a very low contrast belt of equatorial spots may be an artefact due to gravitational darkening.

### *3.3. Mapping procedure*

The inverse problem for stars with cool spots amounts to solving the integral equation relating the surface temperature distribution to the observed line profiles and light and color curve variations, while controlling the effects of noise in the data through a regularizing functional. We solve for the photometric continuum variations *simultaneously* with the line profiles, but can handle only two continuum bandpasses per solution. If the spectroscopic phase coverage contains gaps of more than $\pm 30^\circ$ on the stellar surface more weight is shifted to the photometry.

For all maps in this and subsequent papers in this series we apply the Doppler-imaging code described by Rice et al. (1989) and reviewed by Piskunov & Rice (1993) and Rice (1996). We do not claim that our maps are true, e.g., maximum-entropy maps since the generated maps can not simultaneously fit the geometric constraints and get the error of fit down to the level where the O-C is a Gaussian distribution with a sigma of the size of the formal photon statistical error mainly because the external errors are often much larger and more systematic. The current version of the code includes continuous opacity calculations adjusted for temperature variations across the stellar surface and that allows the use of the latest model atmospheres in the calculation of the local line profiles. Further, the code works from local profile tables that are synthesized strips of spectrum of up to 7 Å so that several lines and line blends (up to 20) can be fit simultaneously.

The code fits either *relative* or *absolute* color variations for continuum light in two photometric bandpasses simultaneously with fitting the line profiles. See Rice & Strassmeier (1998) for a more detailed description and a first application. If the absolute photometry switch is turned on, a calibration between the various model atmospheres and the observed broad-band colors must be supplied to the code. Currently, we adopted the B-V vs. $T_{\rm eff}$ calibration of Flower (1996). For all cool and all low-gravity models this is not without significant additional uncertainties for the absolute spot temperatures (see, e.g., Smalley & Kupka 1997 or Buser & Kurucz 1992). Fortunately, if the atomic line param-

**Table 2.** Adopted $\log gf$ values

| $\lambda$ (Å) | Line | $\chi_{\rm low}$ (eV) | $\log gf$ (Kurucz 1993) | $\log gf$ *(adopted)* |
|---|---|---|---|---|
| 6435.004 | Y I | 0.066 | –0.820 | –1.0 |
| 6435.158 | V I | 1.942 | –1.458 | –2.0 |
| 6436.411 | Fe I | 4.186 | –2.460 | –2.51 |
| 6437.640 | Eu II | 1.320 | –0.276 | –0.45 |
| 6437.703 | Si I | 5.863 | –2.910 | –2.35 |
| 6437.992 | Ni I | 5.389 | –2.984 | –1.50 |
| 6438.088 | V I | 2.684 | –2.070 | –0.30 |
| 6438.755 | Fe I | 4.435 | –2.429 | –2.48 |
| 6439.075 | Ca I | 2.526 | +0.470 | +0.47 |
| 6439.554 | Fe I | 4.473 | –4.304 | –3.55 |
| 6439.705 | Ti I | 0.813 | –6.458 | –6.46 |
| 6440.566 | Si I | 5.616 | –2.480 | –3.28 |
| 6440.938 | N I | 11.764 | –1.140 | +0.5: |
| 6440.971 | Mn I | 3.772 | –1.238 | –1.24 |
| 6441.780 | Fe I | 5.033 | –2.528 | –3.0 |
| 6442.777 | Si I | 6.125 | –1.240 | –4.0: |

eters are basically correct, it is the line strength that determines the surface temperature, not the photometry.

Collier-Cameron (1995) noticed a strong dependence of the recovered total spotted area when the $\chi^2$ of the solution was pushed progressively lower. This is simply because the MaxEnt code will start to overfit the line profiles and produce spurious features on the surface once a critical $\chi^2$ level has been past. Our code is less prone to this problem because we remove the very high frequency noise prior to inversion and therefore do not pre-set the $\chi^2$ level. Solving also for the light curve, as we do, helps to minimize this effect. Although we do not input the overall light and continuum level of the star when "relative" photometry is used, the overall area of the spots is in any case mainly determined from the line shape and strength and while the result – including the total spotted area – is subject to external errors in the line profile data, it should be reasonably correct.

Our program is divided into two main sections. The first block contains the computation of the local line profiles and the minimization and geometry routines. We compute local line profiles from a solution of the equation of transfer from LTE model atmospheres. For HD 199178 a grid of model atmospheres between $T_{\rm eff}$ = 3500 and 6000 K in steps of 250 K and $\log g$ = 2.5 were taken from the ATLAS-9 CD (Kurucz 1993). The gravity of $\log g$ = 2.5 was chosen because a recent determination of the quiet atmospheric structure of the G8III-IV component of the RS CVn binary $\lambda$ And by Donati et al. (1995) yielded such a low value. Maps computed with $\log g$ = 3.0 differ only by their average surface temperature being ≈30 K warmer. For each model atmosphere local line profiles are computed with a wavelength spacing of 0.008 Å. The adopted values for microturbulence and radial-tangential macroturbulence are listed in Table 3 and were taken primarily from the work of Gray (1992). Wavelength-dependent limb darkening is implicitly accounted for during the disk integration.

The second program block is for solving the inverse problem by using either a Maximum-Entropy penalty function or a Tikhonov regularization (for a comparison see, e.g., Collier-Cameron 1992). For all maps in this paper we chose a Maximum-Entropy reconstruction but a Tikhonov reconstruction would be equally suited. The grid spacing for the disk integration is chosen such that each grid element on the stellar surface has equal angular extent in longitude and latitude; in our case $5^\circ \times 5^\circ$.

## 4. Astrophysical parameters of HD 199178

### *4.1. HIPPARCOS-based absolute parameters*

The Hipparcos spacecraft measured a trigonometric parallax of 0.01068″ (ESA 1997) corresponding to a distance of 94±6 pc. The brightest V magnitudes observed between 1975 and 1996 were $7\overset{\rm m}{.}05$ in 1986.84, and $7\overset{\rm m}{.}09$ in 1993.44 and 1993.71 (Jetsu et al. 1999b). Because the $7\overset{\rm m}{.}05$ value is from a single V light curve being on average $0\overset{\rm m}{.}1$ brighter than a light curve taken just one month before, we conservatively adopt the $7\overset{\rm m}{.}09$ brightness as the unspotted (or least-spotted) magnitude. Combined with the distance, this gives an absolute visual magnitude of $+2\overset{\rm m}{.}22\pm0\overset{\rm m}{.}14$. Adopting the bolometric correction of −0.184 from Flower (1996), and neglecting interstellar absorption, we find a bolometric magnitude of $+2\overset{\rm m}{.}04$ and a luminosity of 10.9±2.6 $L_\odot$ (based on $M_{\rm bol,\odot}$ of $+4\overset{\rm m}{.}64$). These properties are typical for (sub)giants of spectral class mid G. The position of HD 199178 relative to the evolutionary tracks of Schaller et al. (1992) for solar metallicity suggests a mass of 1.65 $M_\odot$ with a formal uncertainty of ±0.1 $M_\odot$.

**Table 3.** Stellar parameters for HD 199178.

| Parameter | Adopted |
|---|---|
| Spectral type | G5III-IV |
| Distance | 94±6 pc |
| Luminosity | 10.9±2.6 $L_\odot$ |
| Mass | 1.65±0.1 $M_\odot$ |
| Radius (from $v_{\rm eq}$ and $P_{\rm rot}$) | 7.3±2.2 $R_\odot$ |
| $\log g$ | $< 2.5$–$3.0 >$ |
| $T_{\rm phot}$ | 5450±100 K |
| B-V | 0.78 mag |
| $v \sin i$ | 71.5±1 km s$^{-1}$ |
| Inclination $i$ | 40°±10° |
| Rotation period in 1997 | 3.3286±0.0005 days |
| Micro turbulence $\xi$ | 2.0 km s$^{-1}$ |
| Macro turbulence $\zeta_{\rm R} = \zeta_{\rm T}$ | 4.0 km s$^{-1}$ |
| $\log[Ca]$ abundance | solar |
| $\log[Fe]$ abundance | solar |

### *4.2. Spectral classification and photospheric temperature*

The spectral type was already determined by Herbig (1958) to be G5III-IV. More recently, Huenemoerder (1986) suggested that a classification of G7III-IV would be a better match for the optical spectrum. Although the Hipparcos-based luminosity is consistent with the G5III-IV classification, we point out that there exists considerable uncertainty for the effective surface temperature and gravity of a star of this type. While Bell & Gustafsson (1989) list $T_{\rm eff} = 5600$ K and $\log g$=3.5 for a G5III-IV star and $T_{\rm eff} = 4960$ K for a G8III-IV star (each based on a single star: $\delta$ CrB and $\theta$ Aqr, respectively), Jetsu et al. (1990a) estimated values for HD 199178 in the range of 5300 to 5450 K from broad-band photometry. Recently, Donati et al. (1995) found that the quiet atmospheric structure of $\lambda$ And (G8III-IV) has $T_{\rm eff} = 4750 \pm 30$ K and $\log g = 2.5 \pm 0.2$. We experimented with all these temperatures and found the best fits for the line profiles and the BV(RI)$_c$ photometry when using a nominal photospheric temperature in the range 5400–5500 K and $\log g$=2.5 but allowing the inversion program to freely choose temperatures of up to 6000 K. Finally, we adopted $T_{\rm eff} = 5450$ K as the photospheric temperature that is most consistent with the observed colors and the G5III-IV classification. Note though, that this is not a constraint on the obtainable surface temperature distribution in the mapping process but is the default temperature of the unspotted photosphere.

Jetsu et al. (1990a, 1999a) observed systematic changes of the B-V color between extrema of $0\overset{\rm m}{.}73$ in 1987 and $0\overset{\rm m}{.}83$ in

1981. After 1988/89, the B-V color remained constant to within $\pm 0\overset{\mathrm{m}}{.}02$ and agrees with the Hipparcos B-V of $0\overset{\mathrm{m}}{.}785 \pm 0\overset{\mathrm{m}}{.}015$. Average values for U-B, B-V, V-$R_c$, and V-$I_c$ during the times of our spectroscopic observations in 1988–1990 are $0\overset{\mathrm{m}}{.}30$, $0\overset{\mathrm{m}}{.}78$, $0\overset{\mathrm{m}}{.}45$, and $0\overset{\mathrm{m}}{.}86$, respectively (Heckert & Stewart 1992, Heckert 1994). Comparing these average colors with the theoretical color library generated by Buser & Kurucz (1992) we find reasonable good matches with $(T_{\rm eff}, \log g, [M/H])$ = (5000–5250, 2.5–3.0, −0.5–0.0), but not for 5500 K. In fact, the observed colors do not agree with any $\log g$=2.5–3.0 Buser & Kurucz model *hotter* than $T_{\rm eff} \approx 5250$ K, even if metals were overabundant by 0.5 dex. However, newer tables of (B-V) vs. $T_{\rm eff}$ from the Kurucz (1993) CD-ROM seem to agree much better: for a giant with $\log g \approx 2.5$ and 5500 K a B-V of 0.77 is listed, in good agreement with the observations.

### *4.3. The quest for the correct rotation period*

An uneven spot distribution on the surface of a rotating star allows, in principle, a precise measurement of the stellar rotation period. However, in case the stellar surface is not rigidly rotating the photometric period is a function of the *a priori* unknown latitudinal position of the spots. Differential surface rotation could alter the photometric period by, say, plus-minus several percent. In case of a synchronized binary one can circumvent this problem by using the orbital period as a timekeeper. In case of a single star there is no orbital period and one usually adopts the average photometric period as the stellar rotation period.

Previous determinations for HD 199178 yielded following periods: 3.337±0.001 days (Bopp et al. 1983) from Cloudcroft data taken between June and August 1980; 3.289 days (Nations & Seeds 1986) from Phoenix APT data from 144 nights in late 1985, and 3.337484 ±0.000043 days from a combined data set spanning from 1975 to 1989 (Jetsu et al. 1990a). Instead of the traditional constant period ephemeris, Jetsu et al. (1999a) adopted time-restricted data sets due to sudden phase shifts ("flip-flops") and determined seasonal periods from a large collection of data between 1975 and 1996. Their analysis yields a large and homogeneous set of photometric periods that can be used to phase our spectroscopic data from 1988–1990. The 1996/97 photometry from our own APTs is used to determine the period and light-curve minimum for April 1997 (Strassmeier et al. 1999).

The spectroscopic and photometric data sets in this paper are therefore phased with the following ephemeris: data-set *August 1988*:

$$2,447,276.735 + 3.3279 \pm 0.0009 \times E\ , \quad (1)$$

data-sets *April 1989* and *May-June 1989*:

$$2,447,642.566 + 3.3222 \pm 0.00056 \times E\ , \quad (2)$$

data-set *May 1990*:

$$2,448,014.465 + 3.3147 \pm 0.0017 \times E\ , \quad (3)$$

and data-set *April 1997*:

$$2,450,540.741 + 3.3286 \pm 0.0005 \times E\ , \quad (4)$$

where the period is the seasonal photometric period and the initial epoch is a time of minimum light.

### *4.4. Rotational, radial, and space velocities*

Herbig (1958) was the first to measure the projected rotation velocity, $v \sin i$, of HD 199178 and found 80 km s$^{-1}$. This value was confirmed by Huenemoerder (1986) from comparably low-resolution spectra. More recently, however, Dempsey et al. (1992) obtained $v \sin i$ = 74±2 km s$^{-1}$ from a cross-correlation study using a subset of the NSO spectra from this paper while Fekel (1997) obtained 65.4±5 km s$^{-1}$ from a calibration of FWHM and $v \sin i$.

The inversion of line-profile shapes allows to determine $v \sin i$ even more accurately than with a cross-correlation technique. This is because the line asymmetries due to the spots are modeled explicitly. A wrong $v \sin i$ would produce a pronounced, artificial band encircling the star being either too bright or too dark depending upon whether the adopted $v \sin i$ was too large or too small, respectively (e.g. Vogt et al. 1987). Minimizing such a feature and including the blends from Table 2 yields our adopted value for the projected rotational velocity of 71.5±1.0 km s$^{-1}$.

The mean radial velocity of HD 199178 in the 11 observations from 1997 was $-26.8$ km s$^{-1}$, with a dispersion of 1.4 km s$^{-1}$. The adopted velocity of the reference star $\beta$ Gem was 3.30 km s$^{-1}$. Together with the Hipparcos data, the revised space velocities of HD 199178 relative to the Sun in a right-handed coordinate system are then (U,V,W)=($-9.5 \pm 0.4$, $-26.2 \pm 1.4$, $9.2 \pm 1.0$) km s$^{-1}$.

### *4.5. Inclination of the rotation axis*

Using the rotationally modulated linear Stokes parameters from UBVRI photometry, Huovelin et al. (1987) had derived $i$=79° for the inclination of the rotation axis of HD 199178. This value was later "confirmed" by Jetsu et al. (1990a) by applying the same polarisation model as Huovelin et al. but to a larger data set. Jetsu et al. found inclination angles between 64° and 88° from the first and second-order Fourier fits to the polarimetric variations, respectively. The weighted mean cited by Jetsu et al. (1990a) was 82.2°±1.2°.

We tried inclination angles between 5° and 85° for the line profile inversion and found a significantly larger reduction of the sum of the squares of the residuals (at maximized entropy) when an inclination of 30–50° was used (Fig. 2) instead of 80° as obtained from the polarization measurements. A low value such as this for $i$ has already been suggested by Huenemoerder (1986) on the basis that the equatorial rotational velocity of HD 199178 is less than or equal to that of FK Comae (160 km s$^{-1}$) and that the minimum radius is still in agreement with a G5–7 giant or subgiant spectrum. Our revised values for $v \sin i$ and $P_{\rm rot}$ in 1997 (Table 3) result in a minimum radius for HD 199178 of $R \sin i = 4.70 \pm 0.07\ R_\odot$. If $i \approx$40° is the correct inclination as indicated in Fig. 2, the unprojected radius of HD 199178 is $\approx$7.3 $R_\odot$, i.e. fully consistent with the G5III-IV classification.

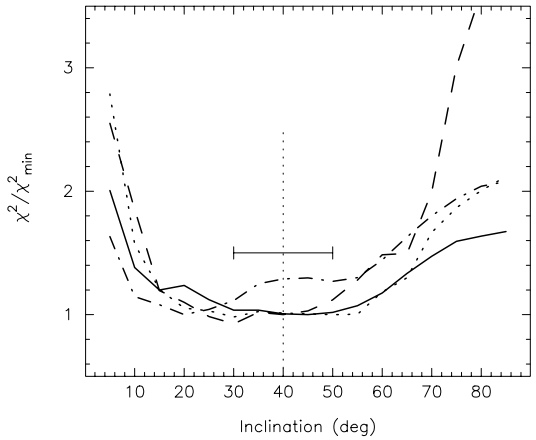


**Fig. 2.** The dependence of the normalized goodness of fit ($\chi^2$) on the adopted stellar inclination angle as discussed in Sect. 4.5. The different line styles are for the different data sets: 1997 (full line), 1990 (dashed line), 1989b (dashed-dotted), and 1989a (dotted line). The inclinations within the horizontal bar give overally the largest reduction of the residuals and we adopt $i = 40^\circ$ as the most likely inclination for HD 199178.

The unprojected equatorial rotational velocity $v_{\rm eq}$ would then be 111 km s$^{-1}$, which is also consistent with HD 199178 being a (rapidly-rotating) FK Comae star.

Both previous polarimetric determinations of the inclination angle were based on the polarization model of Brown et al. (1978). This model is only applicable to pure Thompson or Rayleigh scattering or to a combination of these sources. However, as pointed out by Jetsu et al. (1990a), the wavelength dependence of the amplitude of the rotational modulation of polarization in HD 199178 does not support pure Thompson or Rayleigh scattering but could be accounted for by the Zeeman effect in magnetic surface regions. Also, Jetsu et al.'s values for $i$ derived from the first and second order Fourier fits deviated systematically from each other. As Jetsu et al. noted in their paper, "This discrepancy could be a sign of a yet unexplained pitfall in the method".

Therefore, we believe that the observed polarization variations in HD 199178 are likely caused by a combination of scattering *and* the Zeeman effect due to magnetic surface features rotating in and out of view. Such detections are now being made almost routinely with the technique of Zeeman-Doppler imaging (Donati et al. 1997) and could be used to verify the nature of the polarization variability of HD 199178. Furthermore, there is still a strong controversy about the reliability of broad-band linear polarisation measurements on active stars (Leroy & LeBorgne 1989).

## 5. Discussion of the individual maps

### *5.1. Doppler image for April 1997*

Fig. 3 presents the results from the April 6–16, 1997 data set. Eleven spectra were available along with 31 VI-band light curve points. The combined sum of the squared residuals from the fit

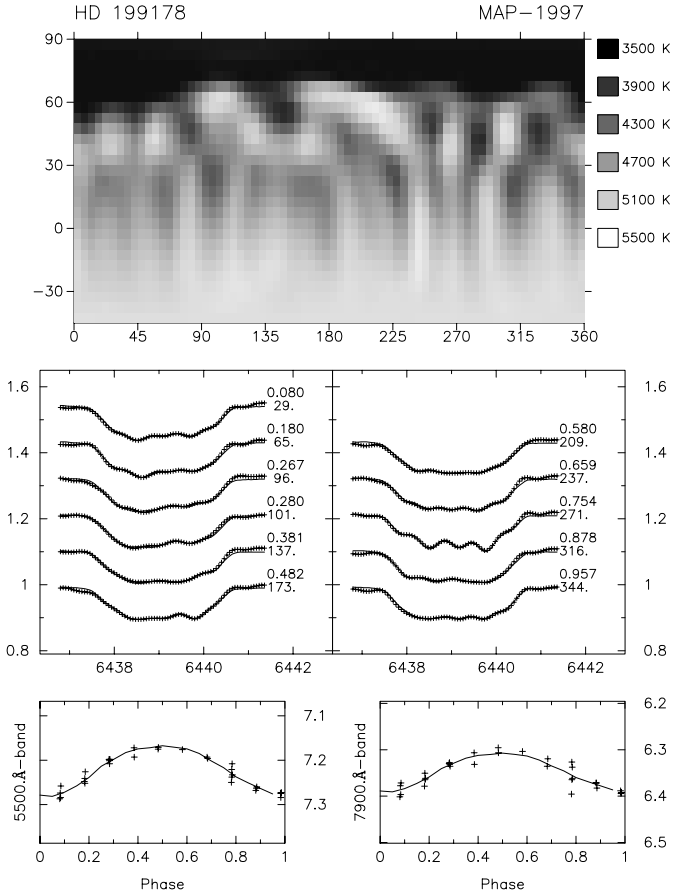


**Fig. 3.** Doppler image of HD 199178 for the observing epoch April 1997. The map in the top panel is shown in a pseudo mercator projection and plots temperature as a grey scale. Zero longitude corresponds to rotational phase zero and is increasing from left to right. The middle panels show the observed (plusses) and computed (line) line profiles, and the lower panels show the absolute photometry in two bandpasses (V and I) and their respective fits.

to the line profiles and the photometry was 0.0152 for the final solution.

The map is dominated by a large and very cool polar spot. It appears asymmetric in shape as well as in its temperature distribution and is the main cause of the light curve minimum at phase zero. The average polar temperature is 3750±100 K (rms), and thus ≈1700 K below the unspotted photosphere. Five appendages of the polar spot are seen in the map. We name these features $P_1 - P_5$ with longitudes, $\ell$, of $\approx 10^\circ$, $77^\circ$, $140^\circ$, $225^\circ$ and $300^\circ$, respectively (Table 4). $P_2$ and $P_3$ are of lesser contrast than $P_1$, $P_4$, and $P_5$; having a temperature difference of ≈1000 K. Several low-latitude spots are also recovered but with comparably even lower contrast. It is possible that the weaker of these features are spurious and were introduced by the external uncertainties of our spectra.

Another noteworthy structure in the map in Fig. 3 is the group of spots gathered within a longitude of 225–360°. Its four main features are clearly seen as pseudo emission bumps in the line profiles at phase 0.754 and partially also at 0.659 (Fig. 3).

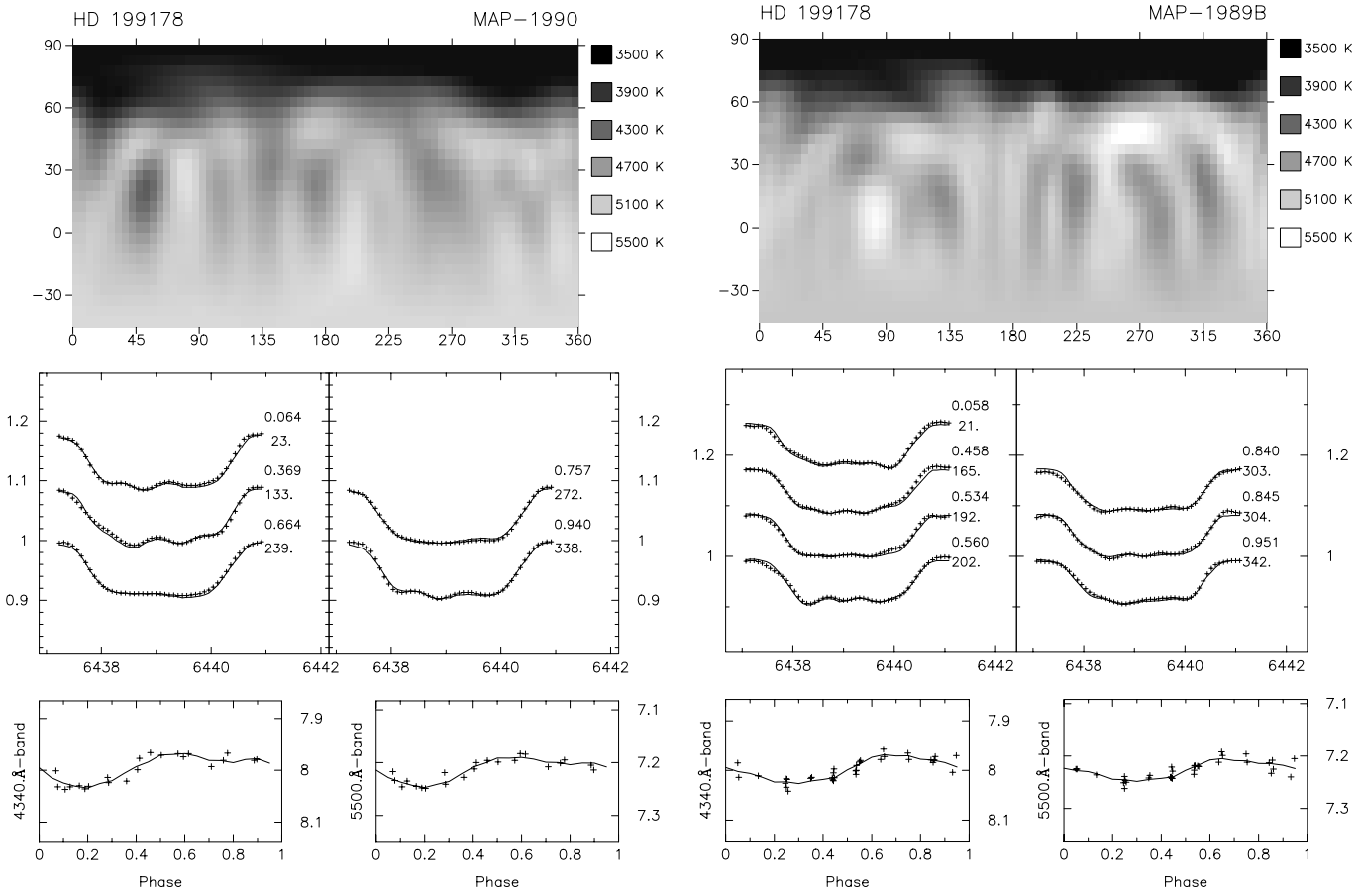


**Fig. 4.** Doppler images of HD 199178 for the four observing epochs 1990 (May), 1989b (May–June), 1989a (April), and 1988 (August). Otherwise as in Fig. 3. All maps were obtained from Ca I 6439 Å and Johnson B (4340 Å) and V (5500 Å) photometry.

The four bumps with amplitudes of 2–3% of the continuum force the code to apply very steep temperature gradients that appear in the map as the adjacent bright and dark features near $\ell \approx 270°$. Despite that the maximum bump amplitudes at this particular phase are nicely fitted with our spot model, the time resolution of our spectra cannot exclude a single, time-variable phenomenon like a local flare-like event.

### *5.2. Doppler image for May 1990*

Fig. 4 ("map-1990") displays the map, the observed and computed line profiles as well as the observed and computed BV-light curve for May 1990. The combined sum of the squared residuals from the line profiles and the photometry was 0.00206 for the final map.

Only five line profiles and 22 BV-data points were available, and such a poor phase coverage will introduce some spurious surface features. Especially suspicious would be those that have low contrast and do not show up in the maps from other lines and are located at very low or even negative latitudes or have a sinusoidal shape across large parts of the image. However, the calcium and iron fits (not shown) have similar $\chi^2$ and the maps agree very well. The only significant difference perhaps is that the small features in the Ca map with $\Delta T \approx 500$ K below $T_{\rm eff}$ are always slightly cooler in the Fe map where some of them appear with $\Delta T \approx 700$ K. The reason for this lies most likely with the different temperature sensitivities of the two lines and possibly also with the uncertain $\log gf$ values, resulting in artificially stronger or weaker mapping lines and thus requiring slightly warmer or cooler spots to fit the profiles equally well.

In 1990, HD 199178 had again a large cap-like polar spot similar to that seen in 1997. We detect two large appendages ($P_1$ and $P_5$) at $\ell \approx 17°$ and 320°, and three weaker appendages ($P_{2,3,4}$) at $\ell \approx 77°$, 140° and 240° (see Table 4). These are basically the same locations as for the five appendages recovered in the April-1997 map seven years later. Besides, six "equatorial" spots were reconstructed at longitudes of approximately 50°, 105°, 138°, 175°, 263° and 330° (called spots $A - F$ in Table 5). The dominating feature at $\ell = 50°$ has a temperature difference of $\Delta T \approx 1200$ K, similar to the polar spot, while the others appear with $\Delta T \approx 800$ K. The combined effect of the large equatorial spot and the polar appendage at $\ell \approx 17°$ is the cause for the light-curve amplitude of $0\overset{\rm m}{.}05$ in V at phase $0\overset{\rm p}{.}20$ (i.e. $\ell \approx 70°$). The APT photometry in Fig. 4 shows the light curve minimum exactly at that phase as well as a broad maximum near $0\overset{\rm p}{.}55 \pm 0\overset{\rm p}{.}05$, and is well matched by the fit from the Doppler image.

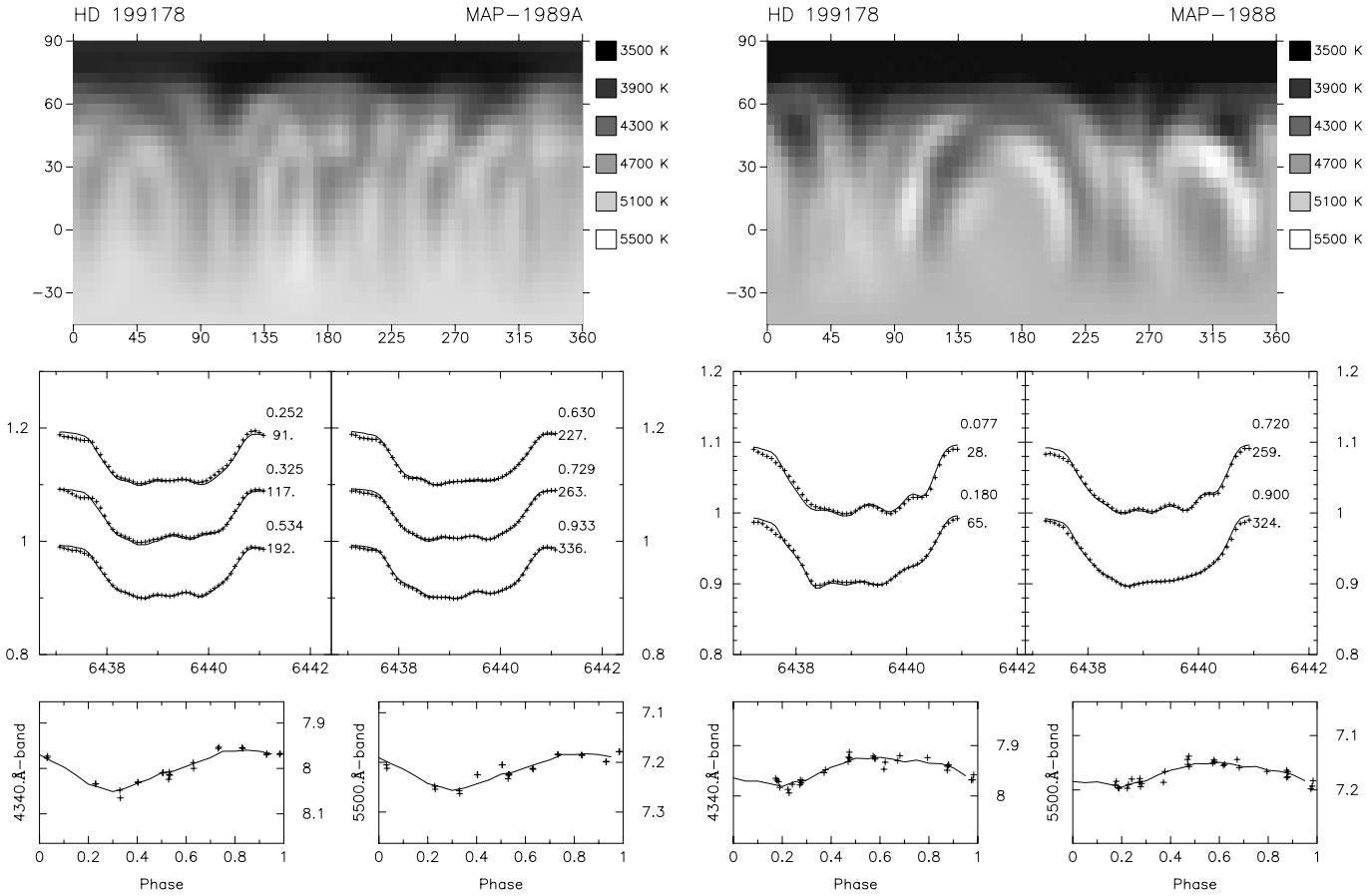


**Fig. 4.** (continued).

### *5.3. Doppler image for May–June 1989*

Seven observations of the Ca I 6439-Å line were obtained between May 25 and June 13, 1989. The map, the line profiles, and the photometry is again shown in Fig. 4 (labeled "map-1989b"). The combined sum of the squared residuals from the line profiles and the photometry was 0.0152 for the final solution.

As in the previous maps, we find a big asymmetric polar spot. The three coolest polar-spot appendages are now $P_3$, $P_4$, and $P_5$, and appear near 180°, 235°, and 330°, respectively. The other appendages, $P_1$ and $P_2$, are still visible at $\ell \approx 30°$ and 107°, respectively, but appear weaker. Both maps, from 1990 and 1989b, indicate a possible connection of $P_1$ with the moderate-latitude spot at $\ell \approx 65°$ and $b \approx$30–40°. The average spot temperature of ≈1300 K below the photospheric temperature is in reasonable agreement with the 1500 K obtained by O'Neal et al. (1996) from TiO-band observations in October 1989. The May-June 1989 map also recovers several low-to-moderate latitude spots or spot groups but with comparably lesser contrast (Table 5) and thus higher uncertainty. It is possible though that these spot groups evolved into the spots recovered in 1990, despite that many of these features are uncertain due to the less-than-perfect phase coverage.

### *5.4. Doppler image for April 1989*

Six observations of the Ca I 6439-Å region were made between April 10 and May 2, 1989. The Doppler image is shown in Fig. 4 (labeled "map-1989a"). The combined sum of the squared residuals from the line profiles and the photometry was 0.00375 for the final map. This map is particularly interesting because it is only one month apart from the previously discussed May–June 1989 map. The effects of time-variable phenomena are thus minimized and a direct comparison allows us to detect short-term evolution of particular surface structures. For example, one of the large polar-appendages ($P_3$) from May–June was either not yet formed one month earlier or significantly smaller, weaker, and sligthly shifted in longitude. The polar cap is still dominating the reconstructed spot distribution, but the now largest and coolest appendage might be a combined $P_4$ and $P_5$ feature with respect to the previous month. The phase coverage at this particular longitude is good and there is no obvious reason for a significant artifact in this surface region. Appendage $P_1$ and the high-latitude spot at $\ell \approx 65°$ and $b \approx +50°$ are merged as compared to May–June where they still appear separated. The phase gap from $0\overset{p}{.}0$–$0\overset{p}{.}2$ causes the reconstruction algorithm to shift more weight to the photometry at these longitudes and thus explains some inconsistencies between the two 1989 maps.

**Table 4.** Longitudinal positions and temperatures of the individual polar appendages

| | $P_1$ | | $P_2$ | | $P_3$ | | $P_4$ | | $P_5$ | |
|---|---|---|---|---|---|---|---|---|---|---|
| Data set | $\ell$ | $T_{\rm min}$ | $\ell$ | $T_{\rm min}$ | $\ell$ | $T_{\rm min}$ | $\ell$ | $T_{\rm min}$ | $\ell$ | $T_{\rm min}$ |
| April 1997 | 10 | 3900 | 77 | 4500 | 140 | 4500 | 225 | 4500 | 300 | 3500 |
| May 1990 | 17 | 3800 | 77 | 4100 | 140 | 4100 | 240 | 4500 | 320 | 3800 |
| May-June 1989 | 30 | 4700 | 107 | 4500 | 180 | 3900 | 235 | 3900 | 330 | 3900 |
| April 1989 | 40 | 4000 | 110 | 4600 | 205 | 3900 | 240 | 3900 | 300 | 4100 |
| August 1988 | 65 | 4300 | ... | ... | 240 | 4150 | 275 | 4300 | 337 | 4300 |

The reidentification of the equatorial spots remains ambiguous because of the large amount of surface detail.

### *5.5. Partial Doppler image for August 1988*

Only four line profiles were available for epoch August 3–10, 1988 and are, together with BV photometry from August through September, used for a *partial* Doppler image (Fig. 4, labeled "map-1988"). The combined sum of the squared residuals from the line profiles and the photometry was 0.00342 for the final map.

This partial image shows again a polar spot very similar to the one discussed in the previous sections. It has four appendages at longitudes of 65°, 240°, 275°, and possibly at 330° that could be identified as $P_1$ and $P_{3-5}$ from the April-1989 map. At this point the reader should be reminded again that the interpretation of spatial information from a few line profiles is somewhat ambiguous because we can just estimate possible external errors, and other cross-identifications could be equally likely. This is especially true for the low-latitude features because their longitudes are more prone to a coarse phase coverage than the polar features. Intercomparison of maps from different years introduces yet additional uncertainty due to differences in the adopted rotation periods as well as due to intrinsic spot variations.

Nevertheless, our code reconstructed five low-to-mode- rate latitude spots or spot groups at longitudes of 17°, 125°, 220°, 250°, and 320°. These features are severely distorted due to the poor phase coverage but are required by the line-profile data, as can be seen from the quality of the fit, but also by the photometry to explain the broad and asymmetric minimum. The apparently most significant low-latitude spot is the one at 130° whose position, however, falls within the large spectroscopic phase gap; its contrast and latitude are thus most uncertain and should be viewed with caution. A feature at $\ell = 17°$ and at a latitude between 30–60° appears significant but it is not clear whether it is a polar appendage or an isolated spot at medium latitude. Table 5 lists it as an "equatorial" feature.

## 6. Summary and conclusions

Vogt (1988) presented the first Doppler image of HD199178 from observations in 1985 and found a big cool polar cap and one, also rather cool, equatorial spot. Our maps show basically the same morphology but with several "equatorial" spots at a given time. In the following we will discuss the spot lifetimes and the involved variability time scales on HD 199178 in more detail.

**Table 5.** Positions and temperatures of lower-latitude spots or spot groups

| | $A$ | | | $B$ | | | $C$ | | |
|---|---|---|---|---|---|---|---|---|---|
| Data set | $\ell$ | $b$ | $T_{\rm min}$ | $\ell$ | $b$ | $T_{\rm min}$ | $\ell$ | $b$ | $T_{\rm min}$ |
| April 1997 | 65 | 20 | 5100 | 100 | 20 | 5100 | 165 | 20 | 5100 |
| May 1990 | 50 | 20 | 4300 | 105 | 25 | 4900 | 138 | 30 | 4600 |
| May-June 1989 | 65 | 40 | 4700 | 132 | 20 | 4750 | ... | ... | ... |
| April 1989 | 67 | 50 | 4400 | 120 | 25 | 4550 | 185 | 25 | 4400 |
| August 1988 | 17 | 50 | 4400 | 130 | 30 | 4300 | ... | ... | ... |
| | $D$ | | | $E$ | | | $F$ | | |
| Data set | $\ell$ | $b$ | $T_{\rm min}$ | $\ell$ | $b$ | $T_{\rm min}$ | $\ell$ | $b$ | $T_{\rm min}$ |
| April 1997 | 224 | 20 | 4800 | 270 | 20 | 5200 | 313 | 30 | 5000 |
| May 1990 | 175 | 25 | 4650 | 263 | 25 | 4700 | 330 | 15 | 5000 |
| May-June 1989 | 220 | 20 | 4500 | 277 | 25 | 4600 | 315 | 30 | 4600 |
| April 1989 | 227 | 30 | 4950 | 257 | 25 | 4650 | 312 | 30 | 5000 |
| August 1988 | 220 | 30 | 4700 | 248 | 20 | 5000 | 320 | 15 | 4800 |

### *6.1. The low-latitude spots*

The maps in Fig. 3 and 4 indicate a generally weak, but persistent, spot coverage at low latitudes. Only the 1990 map revealed a low-latitude spot with a temperature comparable to that of the polar spot. The lifetime of these features is possibly so short that we cannot follow their evolution and unambiguously distinguish between them based on our mostly annual maps. The average latitude of ≈30° remained the same throughout the baseline of our observations from 1988 through 1997. Unfortunately, Doppler imaging is not capable of reliably reconstructing features that appear "below" the stellar equator at negative latitudes; such features will always be weakly mirrored to higher latitudes. The weaker "northern"-latitude spots may well be artifacts of such mirroring.

Tables 4 and 5 identify the positions ($\ell$ = longitude, $b$ = latitude) and the minimum temperatures, i.e. the temperature in the central region of a feature. Note that the temperatures and longitudes and latitudes just refer to an estimated spot center and were based on our Ca I Doppler maps. The positional precision is likely no better than $\pm(5$–$10)°$, while the minimum temperatures ($T_{\rm min}$) are only good to within, say, 50 K.

When we compare our two maps from 1989, just about one month apart, we see that some rearranging of emerging flux

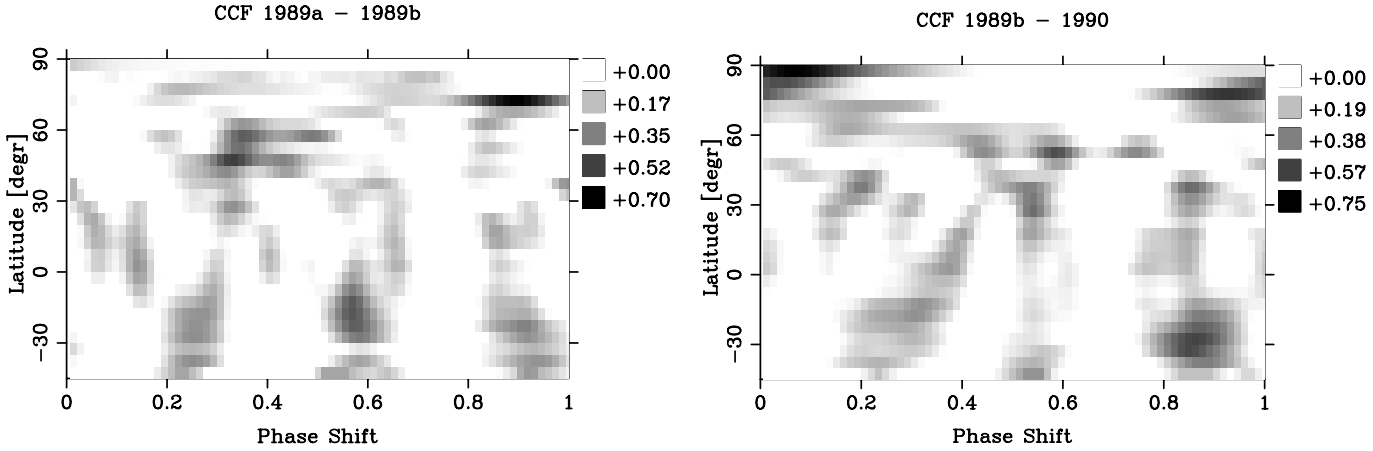


**Fig. 5.** Cross-correlation images. The temperature variation along each 5° latitude bin is cross correlated in the two consecutive maps in 1989 (*left panel*), and 1989b and 1990 (*right panel*). The grey scale indicates the correlation coefficient (from 0 to 1) in the sense that the better the correlation the darker the grey scale. The horizontal axis is the relative phase shifts. Correlations above latitudes of ≈60° and below −20° are only very poorly determined.

at both the polar and the equatorial regions took place. The cross-correlation image in Fig. 5 shows peaks for almost the full range of phase shifts. The individual spots can obviously change fairly rapidly, e.g., the most significant spot (spot $C$) in April 1989 was not seen anymore in May-June 1989, while other features migrated in longitude and/or latitude (spots $A$ and $E$), or remained more or less identical (spots $B$ and $F$), or significantly increased in contrast (spot $D$). Although we have to live with the uncertainty of the spot identification from map to map, it seems clear that the short end of the variability time scale is of the order of one month or even less. This is in agreement with time-series Doppler imaging of other stars, e.g., for EI Eri (Strassmeier et al. 1991, Hatzes & Vogt 1992, Washüttl et al. 1999), or AB Dor (Collier-Cameron & Unruh 1994, Donati & Collier-Cameron 1997).

### *6.2. The polar spot and its appendages*

There is striking evidence for the existence of a polar feature in all our maps in agreement with Vogt's (1988) map from 1985. Nevertheless, we tried several "dirty tricks" to remove the polar cap during our line-profile reconstructions but without much success (see also, e.g., Hatzes et al. 1996). First, we applied various shifts to the continua of all line profiles within a data set to mimic deeper and shallower lines, respectively. Second, the same shifts were applied but with different (integrated) values for the chemical surface abundances as well as microturbulence and macroturbulence velocities. Third, we recomputed local line profiles from a grid of lower and higher $\log g$ model atmospheres ($\log g = 2.0$–$4.0$) in combination with various values for microturbulence (between 0 and 2.5 km s$^{-1}$) as well as relative and absolute photometry. Some of these combinations indeed resulted in a weakening of the polar feature, especially when we neglect microturbulence or adopt too high a $v \sin i$, but none would remove it. We emphasize that blending does not affect our line profile models and therefore cannot account for the existence of the polar feature.

As an additional test, we phased all our line profiles with other photometric periods. None of the periods cited in Sect. 4.3, nor the ones actually adopted (Eqs. 1–4), would remove the polar spot, or produce maps with convincing evidence for the existence of prefered longitudes. This excludes Jetsu et al.'s (1990a) simple model for HD 199178 where starspots form only around two main active longitudes separated by approximately 180°. Just recently, Jetsu et al. (1999a) arrived at the same conclusion from an updated time-series analysis of 20 years of photometry.

Given that the polar spot and its variations are real, we may conclude that its lifetime is at least as long as the time of our observations, i.e. almost nine years. However, it is most likely that we observed the same polar spot that was already seen by Vogt (1988) in 1985. Its overall lifetime would then be at least 12 years. On the contrary, one low-latitude spot seems to have vanished, or at least significantly changed, on a time scale of the order of less than one month.

From a theoretical point of view, a persistent large-scale morphology would be expected because it is predominantly the stellar rotation rate, the field strength in the overshoot layer, and the structure of the convection zone that determine the latitude of emerging magnetic flux (e.g. Schüssler et al. 1996), and these parameters remain stable for a long period of time. From an observational point of view, it is somewhat unexpected though because sudden phase shifts of light-curve minima, as observed for HD 199178 in late 1990 (Jetsu et al. 1999a), are usually explained by the extinction of a particular spot cycle and the begin of a new cycle with new spots at some other longitude (e.g. Berdyugina & Tuominen 1998, Oláh et al. 1997, Henry et al. 1995). This is not what we generally observe on HD 199178. Instead, we see a mixture of the growth and decay of individual features with simultaneous, likely random, redistribution of others; at time scales that are possibly longer for the polar regions. Our inadequate time resolution of basically one map per year

does not permit to follow the evolution of individual features, not even at the pole. However, we strongly suspect that determining an individual starspot's lifetime by simply identifying the beginning and the ending of a consistent light-curve pattern, usually representing just a *constant* migration rate, will grossly overestimate spot lifetimes by up to a factor of 2–5 and possibly even more depending on the rotation rate of the star.

### *6.3. Evidence for differential surface rotation?*

Fig. 5 shows the cross-correlation images for the maps from 1989a and 1989b, and 1989b and 1990. Identifying the highest correlation coefficients, we find mostly more than one significant peak per latitude bin. This ambiguity suggests that the spot distribution changed within our maps. We fitted Gaussians to the most significant peaks of the cross-correlation functions of each latitude bin but found no conclusive evidence for the existence of a consistent migration pattern; neither from our annual Doppler images, nor from the two 1989 maps only one month apart. This is surprising because differential surface rotation is commonly used to explain the observed photometric period variations of spotted stars (Hall 1972, 1996). However, we believe that our non detection does not necessarily mean that there is no differential surface rotation on HD 199178 but merely that its spot distribution is rather dominated by short-term surface field reconnections that mask the differential-rotation signature. A similar result was obtained for the single G8III-II giant HD 51066 (Strassmeier et al. 1998), while consecutive Doppler images of the young K2V-star AB Dor (Donati & Collier Cameron 1997), the K0III giant IL Hya (Weber & Strassmeier 1998) and the T Tauri star V410 Tau (Rice & Strassmeier 1996) gave positive results, indicating solar-like differential rotation. Cases where the polar regions rotate faster than the equatorial zones, i.e. opposite to the solar case, were also found: for V711 Tau (Vogt et al. 1999), UX Ari (Vogt & Hatzes 1991) and HU Vir (Strassmeier 1994, Hatzes 1998); and also from time-series analysis of the Mt. Wilson Ca II H&K data of $\beta$ Com (Donahue & Baliunas 1992). At the moment, Doppler imaging provides no conclusive evidence for differential surface rotation on HD 199178.

*Acknowledgements.* We appreciate the constructive comments and suggestions by the referee, Dr. A. Hatzes, that led to an improved version of this paper. KGS and SL acknowledge the financial support from the Austrian Science Foundation (FWF) under grants S7301-AST and S7302-AST and are grateful to M. Weber for reducing the 1997 spectroscopic data. RCD wishes to acknowledge the help of Drs. Mark Giampapa and Bernard Bopp. JBR acknowledges the financial support from the Natural Science and Engineering Research Council of Canada.

## References

Baschek B., Holweger H., Traving G., 1966, Abh. aus der Hamb. Stw. VIII, No. 1, p. 26
Bell R.E., Gustafsson B., 1989, MNRAS 236, 653
Berdyugina S., Tuominen I., 1998, A&A 336, L25
Bopp B.W., Africano J.L., Stencel R.E., Noah P.V., Klimke A., 1983, ApJ 275, 691
Bopp B.W., Rucinski S.M., 1981, In: Sugimoto D., et al. (eds.) IAU Symp. 93, Fundamental Problems in the Theory of Stellar Evolution. Reidel, p. 177
Bopp B.W., Stencel R.E., 1981, ApJ 247, L131
Brown J.C., MacLean I.S., Emslie A.G., 1978, A&A 68, 415
Buser R., Kurucz R.L., 1992, A&A 264, 557
Choi H.-J., Soon W., Donahue R.A., Baliunas S.L., Henry G.W., 1995, PASP 107, 744
Collier Cameron A., 1992, In: Byrne P.B., Mullan D.J. (eds.) Surface Inhomogeneities on Late-Type Stars. Springer, p. 33
Collier Cameron A., 1995, MNRAS 275, 534
Collier Cameron A., Unruh Y.C., 1994, MNRAS 269, 814
Delbouille L., Neven L., Roland G., 1973, Atlas Photométrique du Spectre Solaire, Université de Liège
Dempsey R.C., Bopp B.W., Strassmeier K.G., et al., 1992, ApJ 392, 187
Donahue R.A., Baliunas S.L., 1992, ApJ 393, L63
Donati J.-F., Collier Cameron A., 1997, MNRAS 291, 1
Donati J.-F., Henry G.W., Hall D.S., 1995, A&A 293, 107
Donati J.-F., Semel M., Carter B.D., Rees D.E., Collier Cameron A., 1997, MNRAS 291, 658
ESA 1997, The Hipparcos and Tycho catalog, ESA SP-1200
Fekel F.C., 1997, PASP 109, 514
Fekel F.C., Balachandran S., 1993, ApJ 403, 708
Fernie J.D., 1991, PASP 103, 1091
Flower P.J., 1996, ApJ 469, 355
Gray D.F., 1992, The observation and analysis of stellar photospheres. Cambridge University Press, p. 243
Hall D.S., 1972, PASP 84, 323
Hall D.S., 1996, In: Strassmeier K.G., Linsky J.L. (eds.) IAU Symp. 176, Stellar Surface Structure. Kluwer, Dordrecht, p. 217
Hatzes A.P., 1998, A&A 330, 541
Hatzes A.P., Vogt S.S., 1992, MNRAS 258, 387
Hatzes A.P., Vogt S.S., Ramseyer T.F., Misch A., 1996, ApJ 469, 808
Heckert P.A., 1994, priv. comm.
Heckert P.A., Stewart M.C., 1992, IBVS 3717
Henry G.W., Eaton J.A., Hamer J., Hall D.S., 1995, ApJS 97, 513
Herbig G.H., 1958, ApJ 128, 295
Huenemoerder D.P., 1986, AJ 92, 673
Huovelin J., Piirola V., Vilhu O., Efimov Y.S., Shakhovskoy N.M., 1987, A&A 176, 83
Jetsu L., Huovelin J., Tuominen I., et al., 1990a, A&A 236, 423
Jetsu L., Huovelin J., Tuominen I., et al., 1990b, A&AS 85, 813
Jetsu L., Pelt J., Tuominen I., 1999a, A&A, in press
Jetsu L., Tuominen I., Bopp B.W., et al., 1999b, A&AS, in press
Keenan P.C., McNeil R.C., 1989, ApJS 71, 245
Kurucz R.L., 1993, ATLAS-9 CD
Kurucz R.L., 1991, In: Davis Philip A.G., et al. (eds.) Precision Photometry: Astrophysics of the Galaxy. Schenectady, Davis, p. 27
Landstreet J.D., 1992, A&AR 4, 35
Leroy J.L., LeBorgne J.F., 1989, A&A 223, 336
Lucy L.B., 1967, Z. f. Astrophys. 65, 89
Moss D., Tuominen I., Brandenburg A., 1991, A&A 245, 129
Nations H. L., Seeds M.A., 1986, IAPPP 25, 56
Oláh K., Kővári Z., Bartus J., et al., 1997, A&A 321, 811
O'Neal D., Saar S.H., Neff J.E., 1996, ApJ 463, 766
Peterson R.C., Dalle Ore C.M., Kurucz R.L., 1993, ApJ 404, 333
Piskunov N.E., Rice J.B., 1993, PASP 105, 1415
Rice J.B., 1996, In: Strassmeier K.G., Linsky J.L. (eds.) IAU Symp. 176, Stellar Surface Structure. Kluwer, Dordrecht, p. 19
Rice J.B., Strassmeier K.G., 1996, A&A 316, 164

Rice J.B., Strassmeier K.G., 1998, A&A 336, 972
Rice J.B., Wehlau W.H., Khokhlova V.L., 1989, A&A 208, 179
Schachter J.F., Remillard R., Saar S.H., et al., 1996, ApJ 463, 747
Schaller G., Schaerer D., Meynet G., Maeder A., 1992, A&AS 96, 269
Schüssler M., Caligari P., Ferriz-Mas A., Solanki S., 1996, A&A 314, 503
Smalley B., Kupka F., 1997, A&A 328, 349
Stift M.J., 1995, priv. comm.
Strassmeier K.G., 1994, A&A 281, 395
Strassmeier K.G., Bartus J., Kővári Z., Weber M., Washüttl A., 1998, A&A 336, 587
Strassmeier K.G., Boyd L.J., Epand D.H., Granzer Th., 1997, PASP 109, 697
Strassmeier K.G., Rice J.B., Wehlau W.H., et al., 1991, A&A 247, 130
Strassmeier K.G., Serkowitsch E., Granzer Th., 1999, A&AS, submitted
Unruh Y.C., Collier-Cameron A., 1995, MNRAS 273, 116
Vogt S.S., 1988, In: Cayrel de Strobel G., Spite M. (eds.) IAU Symp. 132, The Impact of High S/N Spectroscopy on Stellar Physics. Kluwer, Dordrecht, p. 253
Vogt S.S., Hatzes A.P., 1991, In: Tuominen I., et al. (eds.), IAU Colloq. 130, The Sun and Cool Stars: Activity, Magnetism, Dynamos. Springer, Heidelberg, p. 297
Vogt S.S., Hatzes A.P., Misch A., Kürster M., 1999, ApJS, in press
Vogt S.S., Penrod G.D., Hatzes A.P., 1987, ApJ 321, 496
von Zeipel H., 1924, MN 84, 665
Washüttl A., Strassmeier K.G., Collier Cameron A., 1999, A&A, in preparation
Webbink R.F., 1976, ApJ 209, 829
Weber M., Strassmeier K.G., 1998, A&A 330, 1029